*Institute of Space and Aeronautical Science, University of Tokyo*
*Report No. 490, March 1973*

# Current Extension from a Quasi-Steady MPD Arcjet

*By*

Kyoichi KURIKI and Masaaki INUTAKE

*Summary*: Experimental studies were made on the properties of a plasma stream emanating from a pulsed MPD arcjet. From diagnostic measurements, a large fraction of the discharge current was found to extend in the plasma downstream of the electrodes. This extending current was found to be desirable in the quasi-steady operation of an MPD arcjet. The quasi-steadiness should be inferred from the properties of the plasma flow as well as the current and voltage of the arc discharge. The current extension is strongly affected by the working gas injected before the arc discharge, initial tank pressure and applied magnetic field. An instability was found to be induced by the extending current in the plasma plume.

## INTRODUCTION

Pulsed operation of the MPD (Magnetoplasmadynamic) arcjet is an important problem for both practical and fundamental studies of space propulsion. When the MPD arcjet is operated at large discharge current, the electromagnetic effect in plasma acceleration is intensified, and the high thrust efficiency and specific impulse are obtained. The average power and thrust can be controlled by the pulsed operation of variable duty cycle without reducing the thrust efficiency and specific impulse. In the fundamental testing of MPD arcjet, on the other hand, the pulsed operation offers feasibilities in obtaining good vacuum environment and high power level, and in making diagnostic studies. These good features are realized only when the arcjet is operated in quasi-steady state.

From the interests mentioned above, there have been many contributions on the quasi-steady operations of the pulsed MPD arcjet. [*1–9*] The quasi-steadiness of the operation must be judged not only from the operation conditions like the discharge current and the mass flow rate, which may be called external parameters, but also from the properties of the plasma plume like the ion density and velocity, which may be called internal parameters. In the present experiment the emphasis has been placed upon the internal parameters. Diagnostic studies were made in order to find how the quasi-steady operation is affected by the operation conditions.

## EXPERIMENTAL FACILITY AND ITS OPERATION

The pulsed MPD arcjet used in the present experiment has a construction similar to that designed by AVCO Everett Research Laboratory. [*1*] The cross section of

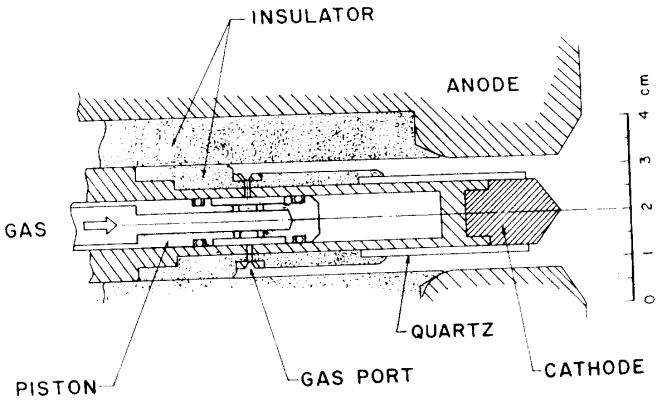


FIG. 1. Cross section of MPD arcjet.

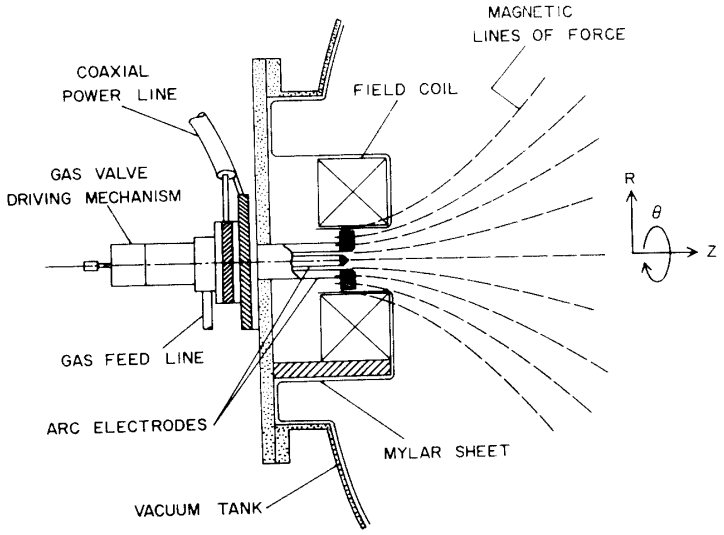


FIG. 2. Schematic of experimental setup.

the arcjet is shown in Fig. 1. The working gas is injected into the annular region between copper anode and tungsten cathode from the gas ports. The gas ports are opened and closed by the sliding O-rings fitted to the piston. The piston is driven by a pre-compressed spring. The mass flow rate is controlled by the inner pressure of the hollow reservoir inside the piston and the total area of the gas ports. The mass flow rate is variable, for instance, from 50 mg/sec to 300 mg/sec for hydrogen. Working gases are hydrogen, helium and argon. A power supply for the arc discharge is a pulse forming network composed of 2,000 $\mu F$ capacitor charged at as high as 5 kV and 100 $\mu H$ inductance.

The MPD arcjet is installed on an end flange of a vacuum tank which is 1.5 m in diameter and 2.8 m in length and made of stainless steel, as shown in Fig. 2. An annular coil is mounted concentric to the arcjet system with its center plane at the anode surface. A power supply for the field coil is 800 $\mu F$ capacitor bank of

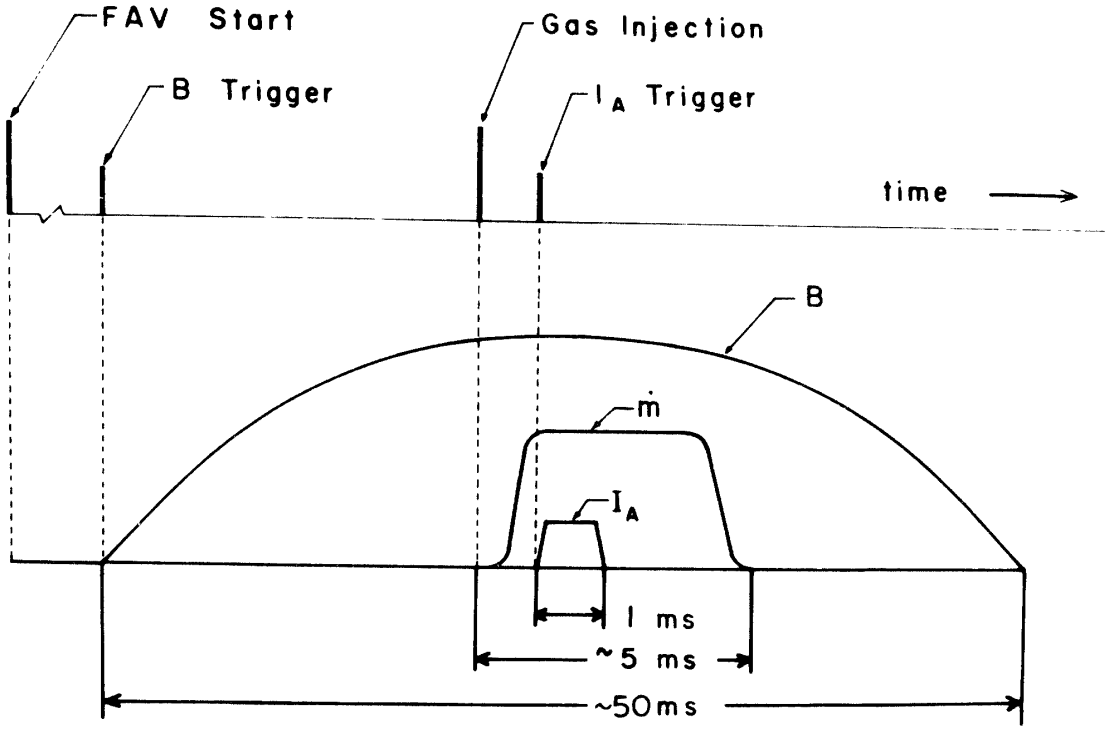


FIG. 3. Time sequence of operation.

5 kV maximum charging voltage and the maximum strength of the magnetic field is 20 kG at the center of the coil. As the anode of the arcjet is grounded together with the tank wall, the inner surface of the tank wall and the metal beds of the coil mount and the traversing mechanism are all insulated by Mylar sheets, in order to prevent the discharge current from flowing in the tank wall. The pressure in the tank is about $10^{-5}$ Torr. A cylindrical coodinate system is taken as shown in Fig. 2.

The time sequence of the normal operation is described in Fig. 3.
The sequences are:

a. The stopper of the compressed spring is released, (FAV Start).
b. The motion of the release mechanism is detected photo-electrically and the signal thus obtained triggers the power supply of the field coil, (*B* trigger).
c. Gas ports are opened, and the mass flow rate becomes constant, (Gas Injection).
d. The piston displacement is detected by a photo-electric device and its signal triggers the power supply for the arc discharge as soon as the mass flow rate becomes constant, ($I_A$ Trigger).

The upper trace in Fig. 4 (a) shows the time variation of the applied magnetic field and the lower trace is the trigger pulse for the arc discharge. The magnetic field can be regarded to be constant during the operation of about 1 msec.

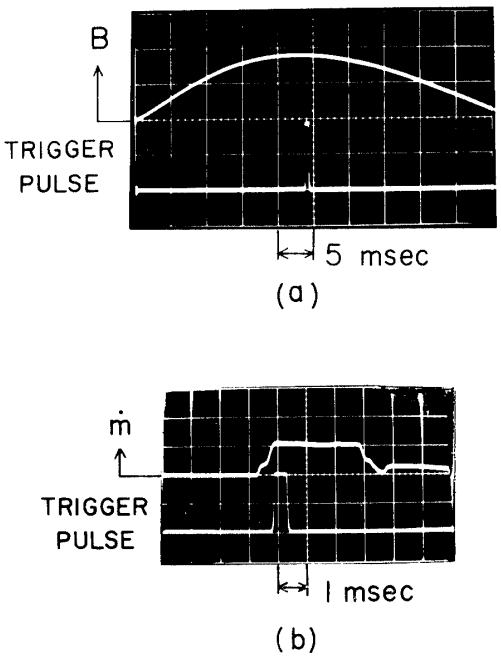


FIG. 4. Trigger timing of arc discharge: (a) applied magnetic field and trigger pulse, (b) output of fast ionization gauge and trigger pulse.

## WORKING GAS INJECTION

The injection of the working gas was studied to determine the trigger time of the arc discharge so that the amount of the neutral gas injected before triggering the arc discharge should be minimized, and to find how a quasi-steady injection of working gas is established in the discharge region. To this end the pressure in the jet of neutral gas was measured by newly developed fast ionization gauge. The gauge has a geometry to cause least obstruction of the flow, and has a sufficient time resolution when cooperated with a constant current circuit. From the calibration in the stationary gas, the sensitivity is found to be constant from $3\times10^{-3}$ Torr to 2 Torr. The detail of the gauge is reported elsewhere. [*10*]

The signal from the ionization gauge, which is proportional to the pressure, is shown in Fig. 4 (b). The gauge is placed at $Z=10$ cm with $Z$-axis taken along the center line and measured from the anode surface. The gas pressure rises in about 600 $\mu$sec after the opening of the gas ports and reaches a constant value. A steady state lasts for 3 msec. The lower trace shows the same trigger pulse as in Fig. 4 (a). From these results together with those in Fig. 4 (a), the time sequence of the operation is found to be achieved as described in Fig. 3.

Fig. 5 demonstrates the time variation of the pressure distribution in the argon jet along the center line. The time origin $t=0$ is taken arbitrarily and the normal trigger time of the arc discharge is 1000 $\mu$sec in this figure. As the time increases, the experimental curve tends to follow a $Z^{-2}$ law. This dependence is predicted from the spherically-expanding steady flow at frozen molecular speed. At the normal

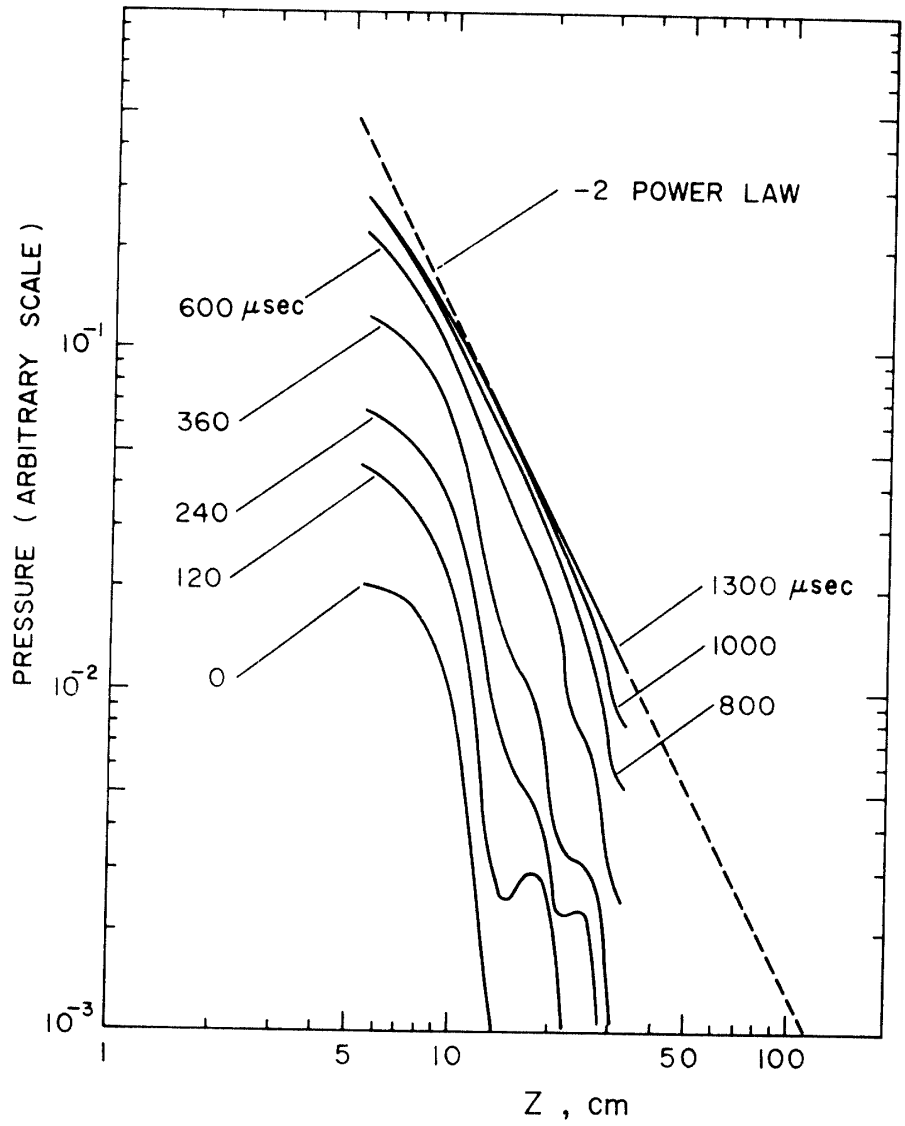


FIG. 5. Time variation of pressure distribution along center line. Argon.

trigger time the steady flow is found to be established as far downstream as $Z=$ 30 cm, where the pressure is about $3\times10^{-3}$ Torr. If an additional 1 msec is elapsed before triggering the arc discharge, the steady flow region is expected to extend as far as $Z=60$ cm. In case of hydrogen and helium, the steady flow is considered to be achieved about three times as fast as in the case of argon because of their faster molecular speeds. As the steady flow region extends downstream, the pressure decrease may level off at the point where it reaches the background pressure $P_t$, which is not shown in Fig. 5. If the working gas continues to be injected more than 3 msec, $P_t$ is increased and the level-off point may shift upstream until the pumping speed will balance the flow rate.

Fig. 6 shows the output of the ionization gauge in the helium jet for various reservoir pressures $P_t$. The five traces in the figure correspond to the reservoir pressures, 1, 2, 3, 4, and 5 atm from bottom to top. Evidently the readings of the

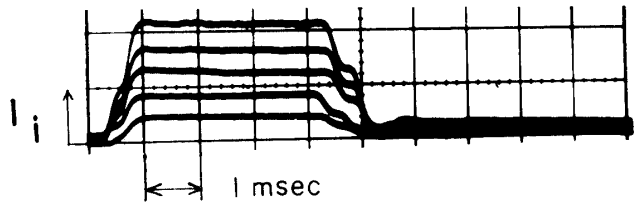


FIG. 6. Output of fast ionization gauge for various reservoir pressures. Helium, $\dot{m}$=0.11, 0.22, 0.33, 0.44, 0.55 g/sec from bottom to top trace, $Z$=10 cm.

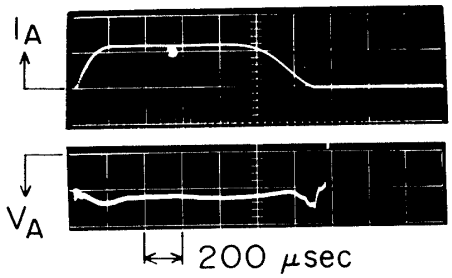


FIG. 7. Current and voltage of arc discharge. Hydrogen, $\dot{m}$=146 mg/sec, $B$=4 kG, $I_A$=12.5 kA. $V_A$: 100 V/div.

output in the steady state are proportional to the reservoir pressures. In the steady flow, therefore, the pressure distribution which is seen to follow $Z^{-2}$ law in Fig. 5 is expected to shift upwards or downwards in proportion to the reservoir pressure.

## CHARACTERISTICS OF ARC DISCHARGE

The electrodes of the MPD arcjet are connected to the pulse forming network together with a series resistance of 150 m$\Omega$. The characteristic impedance of the network is approximately matched with this series resistor and the discharge current is kept constant as long as the arc voltage is much smaller than the voltage drop across the resistor. The upper trace in Fig. 7 is the arc-discharge current and the lower trace is the voltage in a typcal case. The voltage trace represents the cathode potential with reference to the grounded anode. Both of these traces have steady state lasting for more than 800 $\mu$sec. The maximum discharge current is 12.5 kA and the maximum power is about 2 MW. As a conclusion, together with the results of magnetic field and mass flow rate, the quasi-steadiness is found to be achieved for the parameters which can be specified externally.

## ION DENSITY MEASUREMENT

The ion number density, one of the internal parameters, was measured by the Langmuir probe. The probe has a plane surface which is parallel to the flow. The probe is biased strongly negative. A typical trace of the ion saturation current

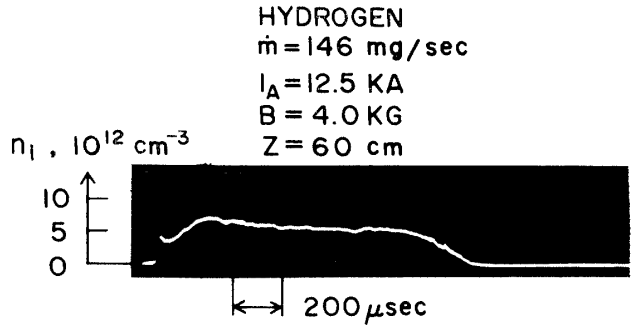


FIG. 8. Ion saturation current of Langmuir probe.

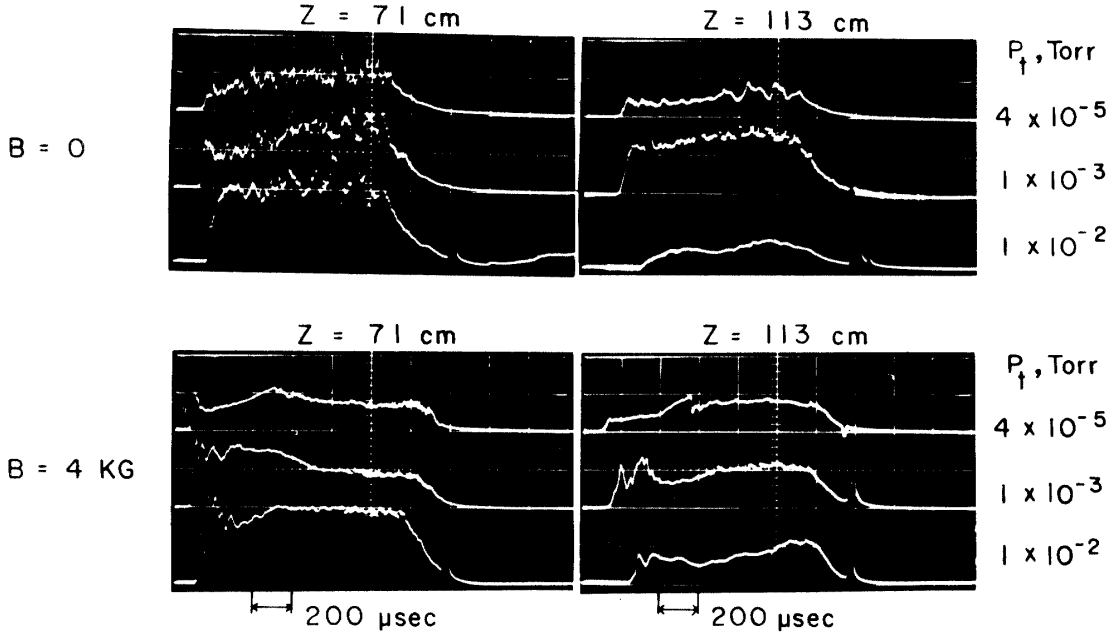


FIG. 9. Ion saturation current of Langmuir probe for various $P_t$, $B$ and $Z$. Hydrogen, $\dot{m}=146$ mg/sec, $I_A=7.5$ kA.

for the normal operation is shown in Fig. 8. The operation conditions are $\dot{m}=$ 146 mg/sec of hydrogen, $I_A=12.5$ kA, $B=4$ kG and $Z=60$ cm. The electron temperature is found to be 4 eV and rather insensitive to the operation conditions.

In Fig. 9 is shown a matrix representation of the ion density trace: the column refers to the probe location and the row refers to the magnetic field $B$. The initial tank pressure is taken as a parameter. The horizontal sweep of the traces is triggered by the pulse that triggers the arc discharge. The time of the plasma front arrival at the probe $\tau_F$ is defined as the moment when the ion density reaches a steady value. The smaller $\tau_F$ simply means a faster speed of the plasma front. Apparently the front speed is slowed down when the tank pressure $P_t$ is raised. In addition, the gradient of $n_i$ at the plasma front becomes gradual when $P_t$ is increased to $10^{-2}$ Torr and the magnetic field is absent. When the magnetic field is applied, not only is the plasma front accelerated but also the ion density rises more

steeply. At $Z=71$ cm noisy fluctuations are superposed on the trace for $B=0$, whereas regular damping oscillations with lower frequencies are observed near the front for $B=4$ kG. The latter oscillations are attributable to the hydromagnetic waves as will be discussed in the next section. Another comment can be drawn from the final part of the trace. The density for $B=0$ begins to fall off the steady value earlier and decays more slowly than that for $B=4$ kG. With an applied magnetic field, the ion density has a longer steady state and falls off more rapidly. From all these effects, the magnetic field is concluded to contribute increasing the duration of steady operation, even when the tank pressure is increased. Note that one vertical division for $B=4$ kG is twice as large as that for $B=0$. The effect of the tank pressure becomes more remarkable at $Z=152$ cm as shown in Fig. 10. At this position the quasi-steadiness is almost lost at the tank pressure above $3\times10^{-3}$ Torr even with the magnetic field of 4 kG. The notation at the top of this figure,

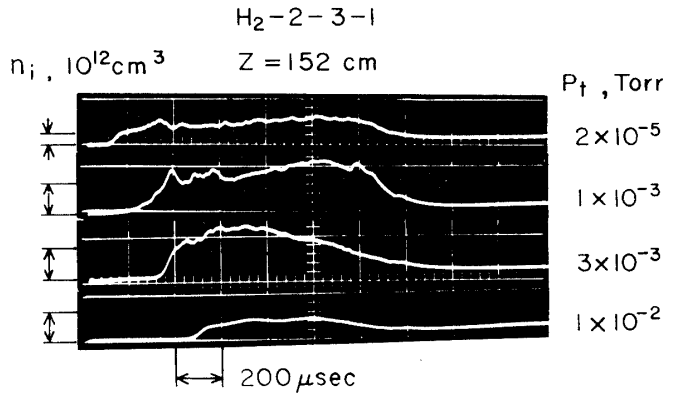


FIG. 10. Ion saturation current of Langmuir probe for various $P_t \cdot Z=152$ cm.

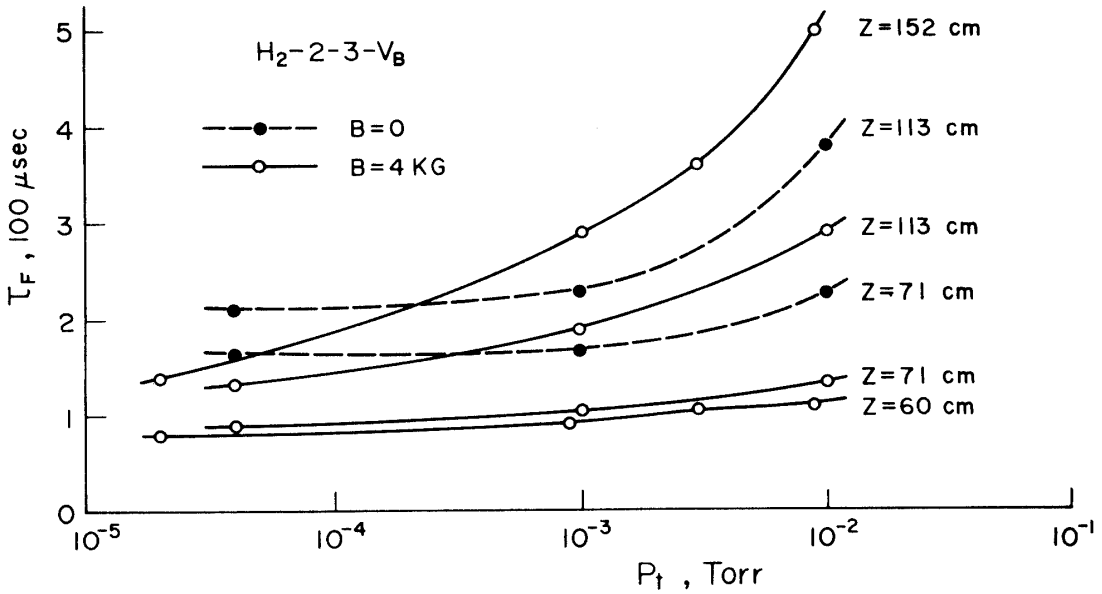


FIG. 11. Effects of initial tank pressure and magnetic field on plasma-front arrival.

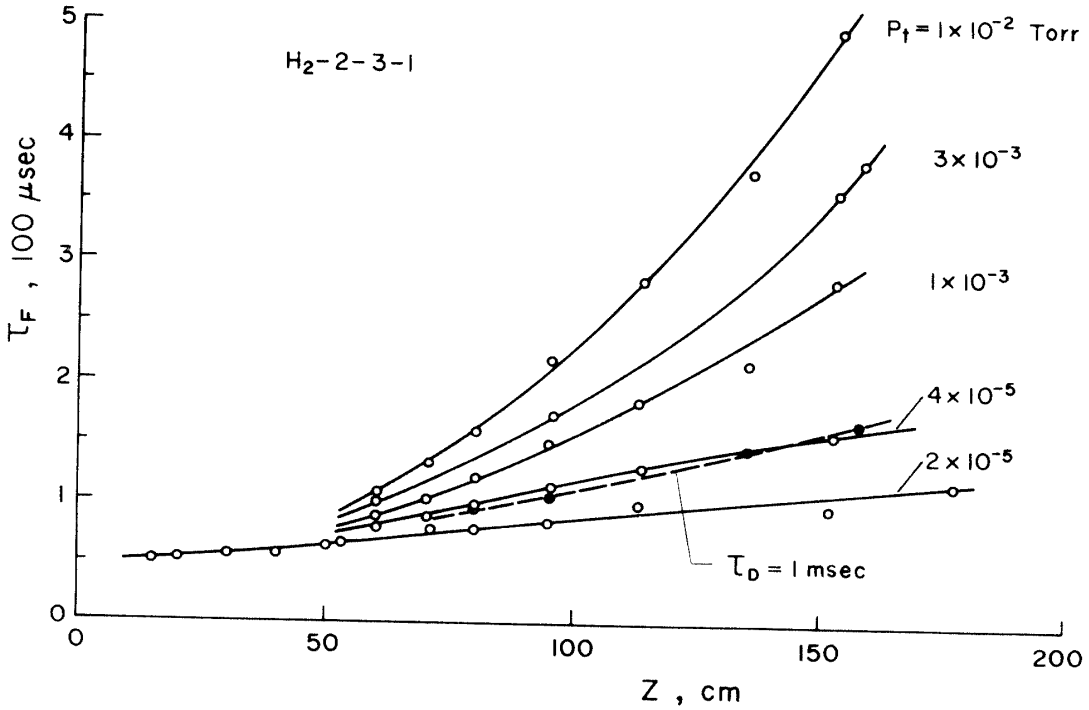


FIG. 12. Effects of initial tank pressure and trigger delay on plasma-front arrival.

$H_2$ -2-3-1, means that the working gas, the reservoir pressure and the charging voltages of the capacitors for the arc discharge and the magnetic field are hydrogen, 2 atm, 3 kV and 1 kV, respectively. Actually these conditions correspond to $\dot{m} =$ 146 mg/sec, $I_A = 7.5$ kA and $B = 4$ kG.

The results of $\tau_F$ measurement are summarized in Figs. 11 and 12. The effects of the initial tank pressure and the magnetic field are evident in Fig. 11. The moment when the ion density falls off the steady value is rather insensitive to the tank pressure and the probe position as can be observed in Fig. 9. The duration of the steady state, therefore, is essentially determined by $\tau_F$. In Fig. 12 the results from magnetic probe measurements, which will be discussed in the next section, are included together with those from Langmuir probe measurements. The results from the two kinds of measurements are quite consistent. When the trigger of the arc discharge is delayed by 1 msec from the normal time, a slight increase in $\tau_F$ is observed as shown in Fig. 12, where $\tau_D$ represents the trigger time delay. From the discussions of working gas injection, the steady flow of the neutral gas is considered to be established as far downstream as $Z \simeq 1$ m for hydrogen even in the normal operation. Therefore, it is reasonable that the effect of the trigger delay becomes significant in the region $Z \gtrsim 1$ m.

The effect of the mass flow rate on $\tau_F$ was found markedly in the ion-density trace. The plasma front arrival observed at $Z = 152$ cm is considerably delayed when $\dot{m}$ is increased from 73 mg/sec to 220 mg/sec. The pressure near the jet exit is raised by the increase of $\dot{m}$ before triggering the arc discharge and the effect on $\tau_F$ is similar to the one by the increased tank pressure.

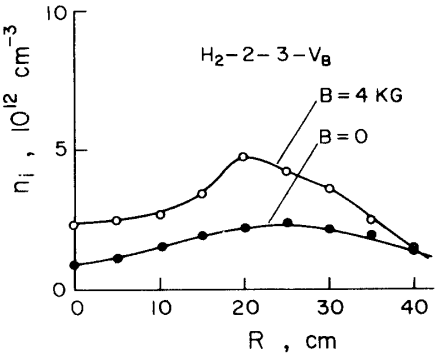


FIG. 13. Radial distribution of ion number density.

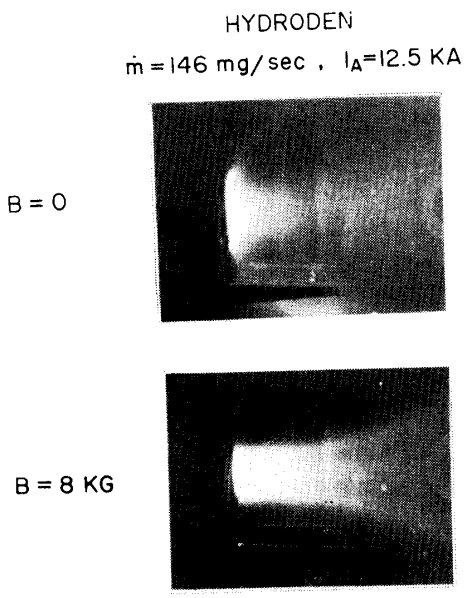


FIG. 14. Time-exposure photographs of plasma plume. Hydrogen.

Fig. 13 shows the radial distribution of the ion density at $Z=71$ cm in the cases with and without magnetic field. The distribution for $B=4$ kG has a prominent maximum at a radial position off the center. In the case of $B=0$ the radial position for the maximum shifts to the outer region when compared with the case of $B=4$ kG. Time-exposure photographs of the plasma plume are shown in Fig. 14 for the cases with and without magnetic field. When the magnetic field is applied, the plasma plume has a structure with central luminous core and outer trumpet-shaped luminous layer. Between the two luminous region a dark region can be observed.

Although the luminosity is not so clear at $Z=71$ cm, the maximum of $n_i$ in Fig. 13 is found to occur approximately in the outer luminous region. When the magnetic field is absent, only a luminous blob is observed just at the exit of the arcjet.

## ARC CURRENT EXTENDING DOWNSTREAM

From the magnetic probe and Rogowski coil measurements, a large fraction of the discharge current was found to flow in the plasma plume. There have been conjectures on the current extrusion, [*11*, *12*] and the results obtained in the present experiment seem to be best explained by the mechanism due to Can. [*12*] From the foregiong results of the ion density it is expected that the plasma front is accelerated by the electromagnetic force induced by the extending current, and that the operation conditions affecting the speed of plasma front might influence the current extrusion.

The azimuthal component of the magnetic field was measured by magnetic probes of 7 mm diameter and 410 turns. The Rogowski coil has 10 cm major diameter.

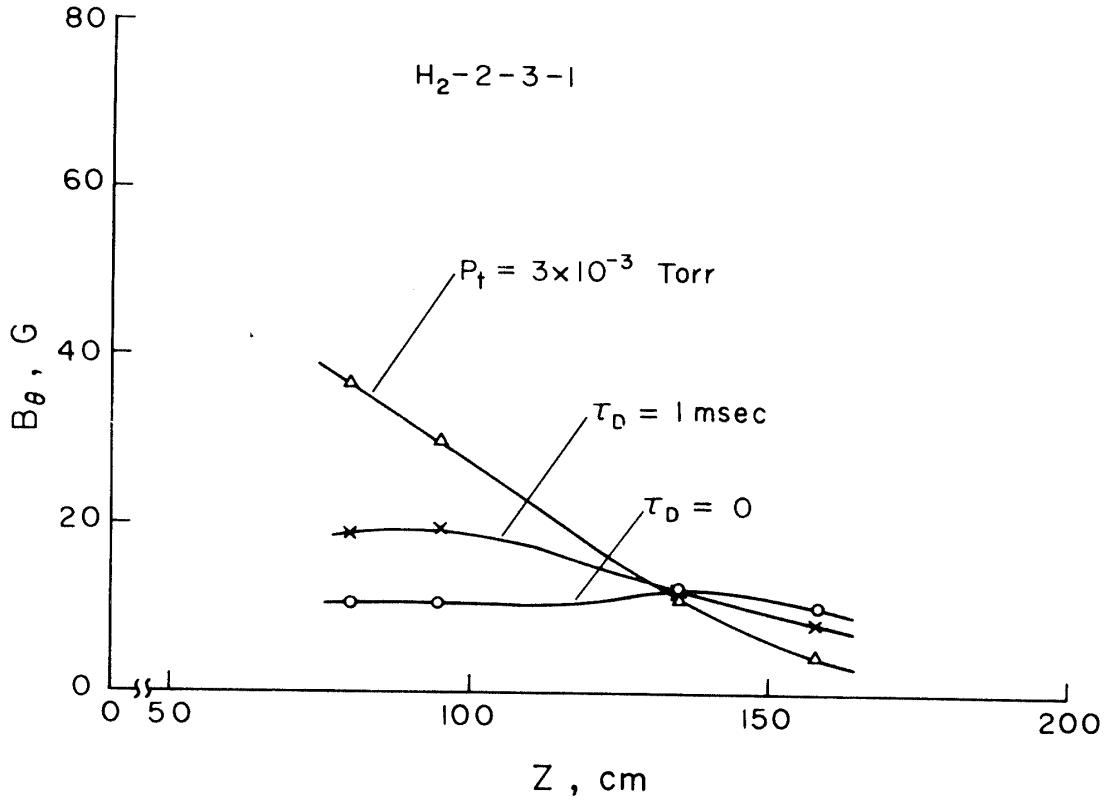


FIG. 15. Effects of initial tank pressure and trigger delay on azimuthal magnetic field. Results for $\tau_D=0$ and $\tau_D=1$ msec are taken at $P_t=2\times10^{-5}$ Torr.

Signals from these coils were integrated by an RC circuit with 10 msec time constant. The absence of the current flowing into the tank wall was frequently checked by a Rogowski coil of 20 cm major diameter which encircles the whole plasma plume.

The azimuthal magnetic field $B_\theta$ measured at $R=5$ cm is plotted against $Z$ in Fig. 15. The magnetic field $B_\theta$ is equivalent to the total current flowing through a circle of 5 cm radius. When the tank pressure is increased, or when the trigger time is delayed, $B_\theta$ increases near $Z=100$ cm and decreases towards downstream more rapidly than in the normal operation. Fig. 16 demonstrates how $B_\theta$ is affected by $P_t$. When the pressure is increased from $2\times10^{-5}$ Torr, $B_\theta$ at $Z\simeq100$ cm increases and takes maximum at $P_t\simeq3\times10^{-3}$ Torr, and hereafter decreases. The radial distribution of $B_\theta$ was measured to find axially extending current and is shown in Fig. 17. Since the maximum value of $B_\theta$ in this figure is equivalent to the extending current, it is concluded that the extending current as far downstream as $Z\simeq100$ cm is the largest at $P_t\simeq3\times10^{-3}$ Torr. The maximum ionization efficiency of electron is found to occur at $E/p=500$ V/cm·Torr for hydrogen, [*13*] where $E$ and $p$ represent the electric field and the neutral gas pressure, respectively. From the measurement of potential distribution the average value of $E$ is found to be about 1 V/cm in the present experiment. Hence the maximum ionization efficiency occurs at $p=2\times10^{-3}$ Torr, which is very close to $P_t$ for the maximum extending current

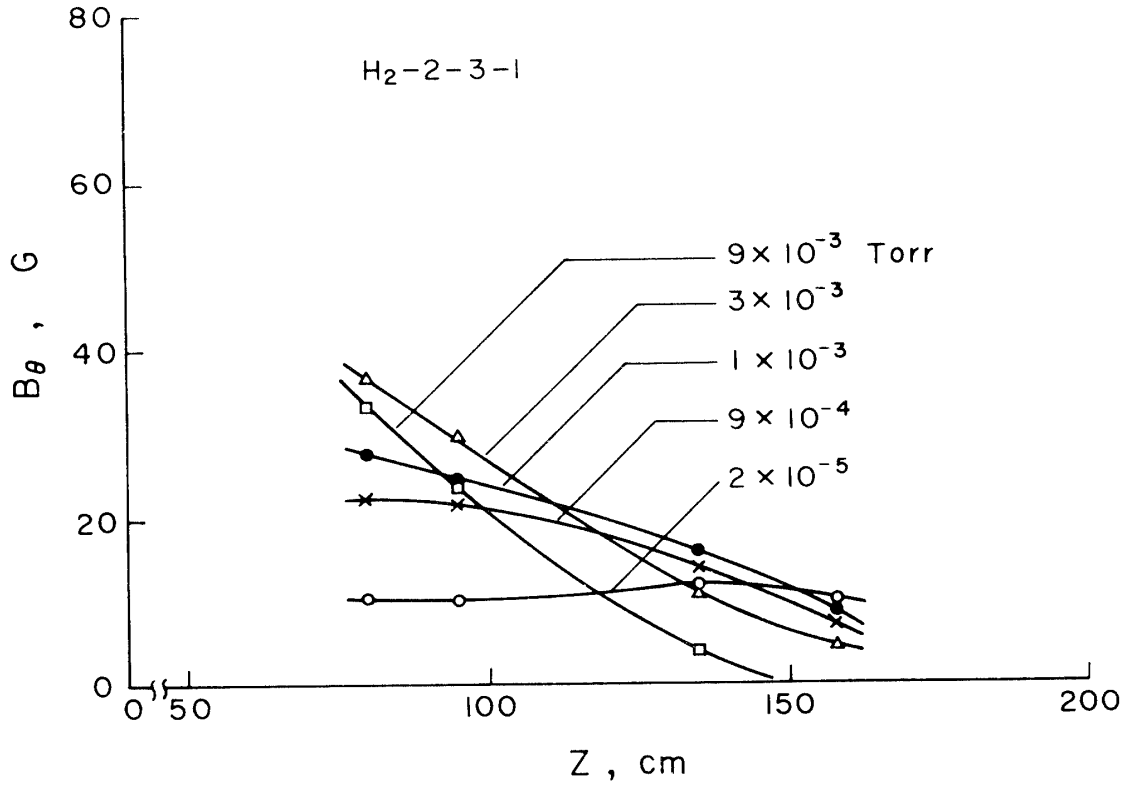


FIG. 16. Effect of initial tank pressure on azimuthal magnetic field.

at $Z\simeq 100$ cm. When the tank pressure is moderately high like $P_t=3\times10^{-3}$ Torr, a large fraction of the discharge current is likely to extend from the arcjet.

If the pre-injected working gas is considered to have an effect similar to the tank pressure, the following process can be expected. The speed of the plasma front can be calculated from Fig. 12 and is 40 km/sec for the normal operation. Hence the diffusing front of the neutral gas, which is moving much slower than the plasma front, is caught by the ionizing front accompanied with the extending current. The pre-injected working gas is thus considered to be ionized and effectively participates in the thrust production.

The maximum $B_\theta$ in Fig. 17 occurs at the slightly inward radial position in comparison with the maximum $n_i$ in Fig. 13. At the position of the maximum $B_\theta$ the current flowing in $Z$ direction reverses its sign and this radial position lies in the dark region in Fig. 14. The extending current, therefore, flows downstream in the outer luminous layer and flows back to the cathode through the central luminous core.

The trace of $B_\theta$ at $P_t=3\times10^{-3}$ Torr is demonstrated in Fig. 18. At the initial part of the trace in this figure, large amplitude oscillations are observed. These oscillations of $B_\theta$ are coupled with the density oscillations found in Fig. 9 and constitute hydromagnetic waves.

The results of $B_\theta$ measurement are transformed into $I_{\mathrm{JET}}$, which is defined as the total current flowing in the region $R\leq 5$ cm. The values thus transformed are plotted

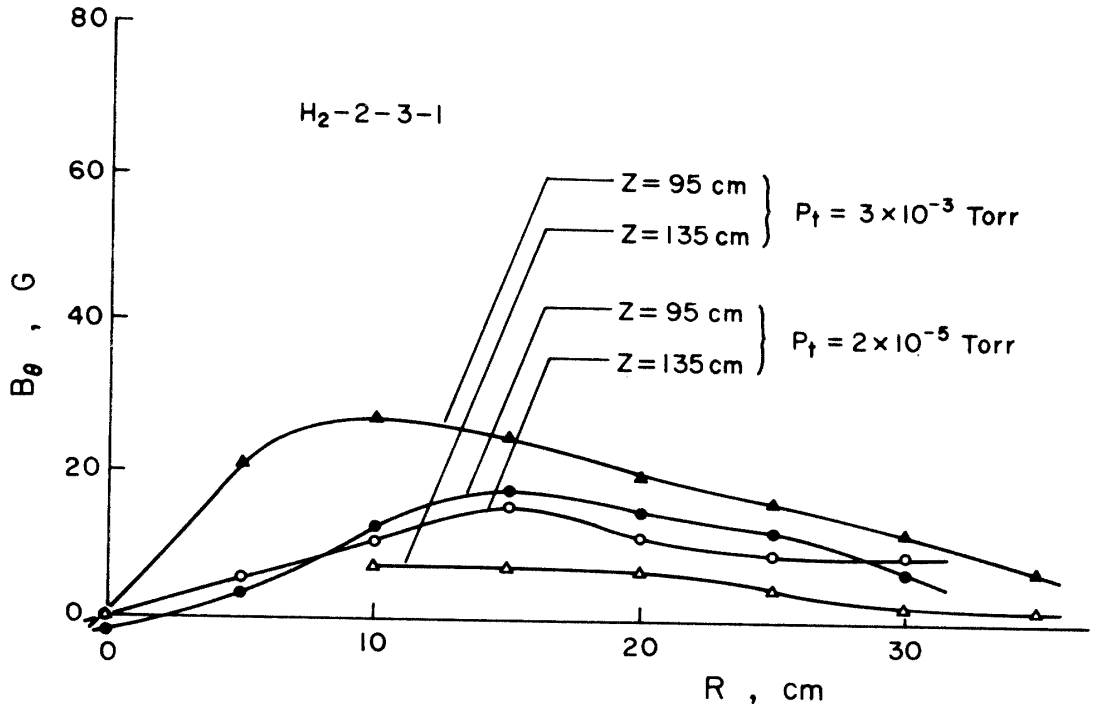


FIG. 17. Radial distribution of azimuthal magnetic field.

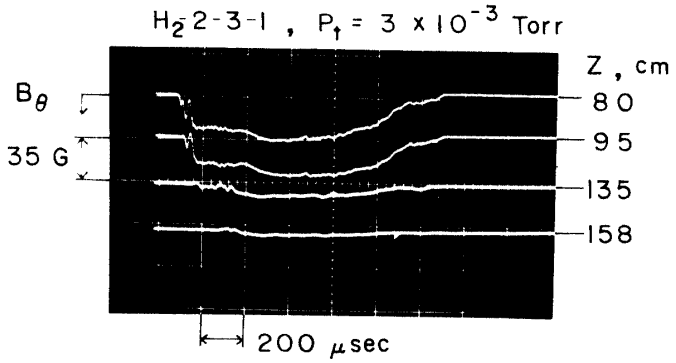


FIG. 18. Aximuthal magnetic field obtained by magnetic probe. $R=5$ cm.

together with the results from the Rogowski-coil measurement, which gives $I_{JET}$ directly. The current $I_{JET}$ is plotted against $Z$ for $B=4$ kG in Fig. 19 and for $B=6$ kG in Fig. 20. Almost 50% of the discharge current extends out of the arcjet when $B=6$ kG. As shown in Fig. 19, the extending cerrent is extremely small even for $I_A=12.5$ kA when the magnetic field is absent. In this case no significant signal was observable on the $B_\theta$ trace obtained in the region $Z \geq 50$ cm.

In Figs. 19 and 20 the vertical spines around the experimental points represent the oscillations of $B_\theta$ superposed on the steady trace. The vertical length of the spine denotes the amplitude of the oscillation. The oscillation grows in the decreasing region of $I_{JET}$, and further downstream saturates in its amplitude and is damped. The trace of $B_\theta$ is shown in Fig. 21. The traces for $B=4$ kG in Fig.

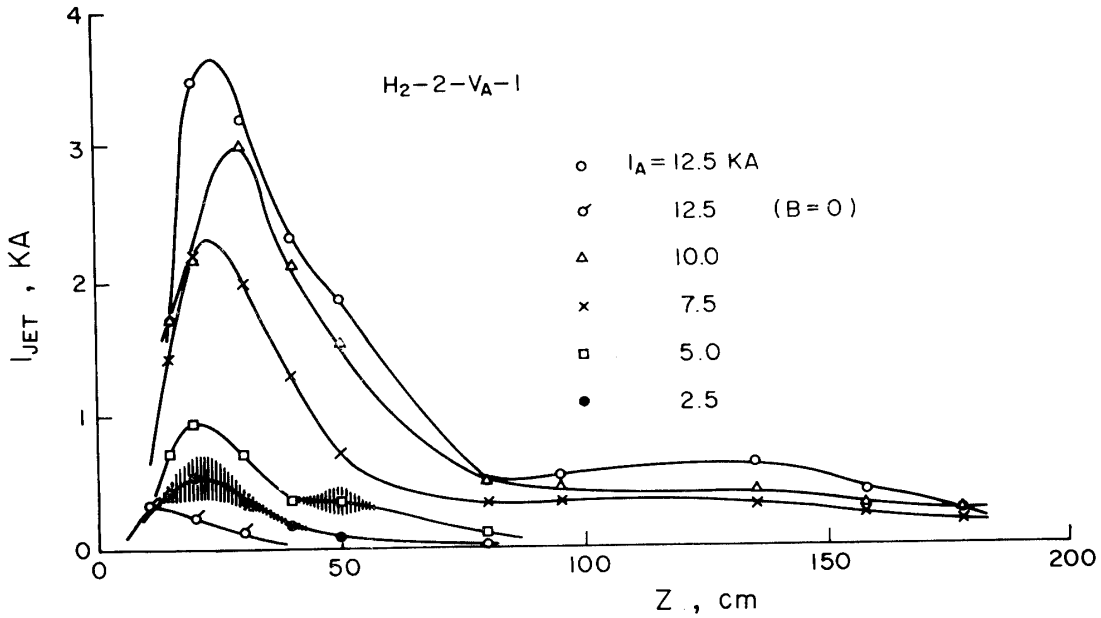


FIG. 19. Arc current extending in plasma plume. $\dot{m}=146$ mg/sec, $B=4$ kG.

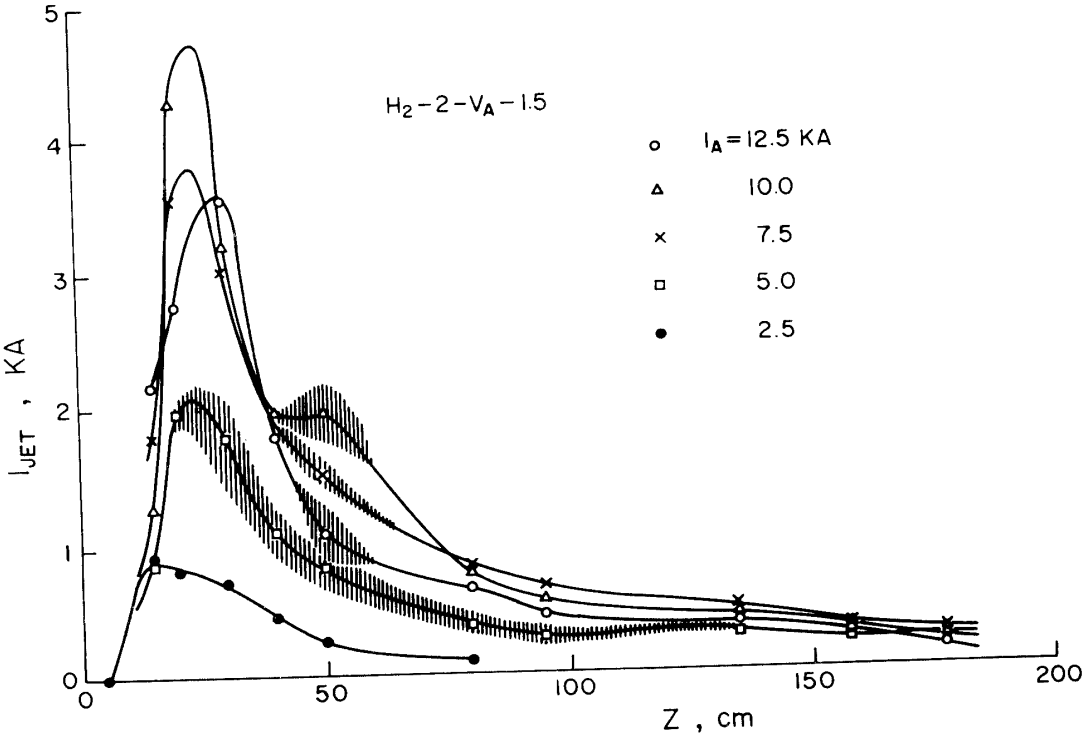


FIG. 20. Arc current extending in plasma plume. $\dot{m}=146$ mg/sec, $B=6$ kG.

21. (a) show good quasi-steadiness and have little oscillation. When the field strength is raised to 8 kG, oscillations appear on the $B_\theta$ traces as illustrated in Fig. 21 (b). The frequency of the oscillation ranges from 20 to 100 kHz. In this range falls the ion cyclotron frequency referred to the strength of the applied magnetic

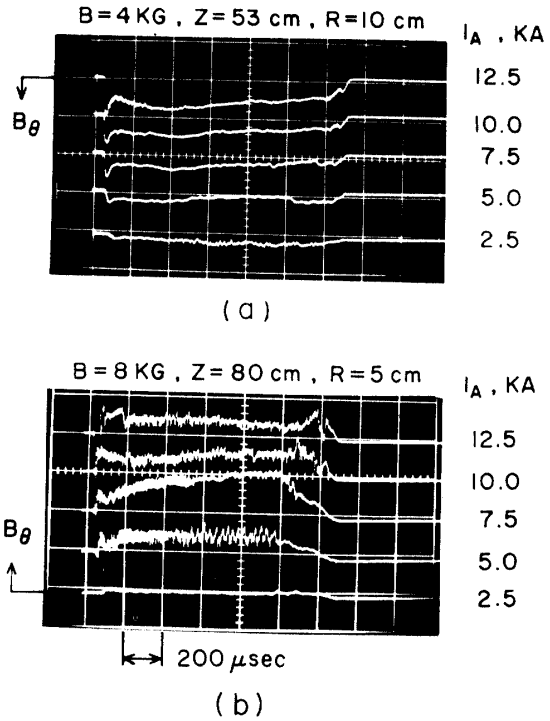


FIG. 21. Aximuthal magnetic field obtained by magnetic probe. $\dot{m}=146$ mg/sec, (a) $B=4$ kG, (b) $B=8$ kG. Vertical scale: 35 G/div.

field or the current-induced self field at $Z\simeq 50$ cm. Since the total amount of the extending current, i.e. the maximum of $I_{JET}$, does not differ greatly for $B=4$ kG and $B=6$ kG, the onset of the instability is not determined by the absolute value of $I_{JET}$, alone, but strongly influenced by the magnetic field strength. Although the mode of the instability could not be identified completely, either the current-driven magnetosonic instability or the drift instability is considered to occur since the extending current density exceeds the threshold value. [*14*] The effect of the instability on the plasma velocity is considered as a future subject of the present experiment.

## ACKNOWLEDGEMENT

The authors would like to express their sincere thanks to Mr. K. Yoda for his engineering assistance througout this work and also to the members of the Machine Shop for their skilled works in constructing the arcjet system and probes.

*Department of Aerodynamics*
*Institute of Space and Aeronautical Science*
*University of Tokyo, Tokyo*
*February 5, 1973*

## Reference

[1] Pugh, E. and Patrick, R.: "Plasma Wind Tunnel Studies of Collision-Free Flows and Shocks", Phys. Fuilds, **10**, 2579 (1967).
[2] Eckbreth, A. C. and Jahn, R. G.: "Current Pattern and Gas Flow Stabilization in Pulsed Plasma Accelerators", AIAA J., 8, 138 (1970).
[3] Clark, K. E. and Jahn, R. G.: "Quasi-Steady Plasma Acceleration", AIAA J., 8, 216 (1970).
[4] Jahn, R. G., Clark, K. E., Oberth, R. C. and Turchi, P. J.: "Acceleration Patterns in Quasi-Steady MPD Arcs", AIAA J. 9, 167 (1971).
[5] Cochran, R. A. and Fay, J. M.: "Occurrence and Behavior of Current Spokes in MPD Arcs," AIAA J., 9, 893 (1971).
[6] Kribel, R., Eckdahl, C. and Lovberg, R., "Properties of the Rotating Spoke in an Unstable Pulsed MPD Arc," AIAA J., 9, 893 (1971).
[7] Michels, C. J. and Sigman, D. R.: "Exhaust characteristics of a Megawatt Nitrogen MPD Arc Thruster", AIAA J., 9, 1144 (1971).
[8] Turchi, P. J. and Jahn, R. G.: "Cathode Region of a Quasi-Steady MPD Arcjet," AIAA J., 9, 1372 (1971).
[9] Hoell, J. M. Jr., Burlock, J. and Jarrett, O. Jr.: "Velocity and Thrust Measurements in a Quasi-Steady Magnetohydrodynamic Thruster", AIAA J., 9, 1969 (1971).
[10] Inutake, M. and Kuriki, K.: "Fast Ionization Gauge Studies of Quasi-Steady Gas Injection into Vacuum", Rev. Sci. Instr., **43**, 1670 (1972).
[11] Schneiderman, A. M. and Patrick, R. M.: "Axial Current Distribution in the Exhaust of the Magnetic Annular Arc," AIAA J., 5, 249 (1967).
[12] Cann, G. L.: "Annular Magnetic Hall Current Accelerator," AIAA Paper 64–670 (1964).
[13] von Engel, A.: *Ionized Gases*, Oxford at the Clarendon Press (1955).
[14] Kadomtsev, B. B.: *Plasma Turbulence*, Academic Press, New York (1965).